Effect of microstructural length scales on crack propagation in elastic Cosserat media

Soukaina Riad, Didier Bardel, Julien Réthoré

Effect of microstructural length scales on crack propagation in elastic Cosserat media

Soukaina Riad[a,b], Didier Bardel[b], Julien Réthoré[a,*]

[a] *Civil and Mechanical Engineering Research Institute (GeM), Centrale Nantes/ Université de Nantes/ CNRS, UMR 6183, 1 rue de la Noë, F-44321 Nantes, France*
[b] *Framatome, 10 rue Juliette Récamier, 69456 Lyon cedex 06, France*

Abstract

This contribution introduces a multiscale fracture model that aims to take the microstructural length scale effects into account in brittle failure. This model is formulated in the framework of Cosserat continuum theory and coupled with the phase field approach to failure to describe complex crack paths. The effectiveness of the proposed method is demonstrated using two cases: a shear crack propagation problem and a crack interaction problem. The first benchmark problem is proposed to reveal the synergistic aspect between Cosserat kinematic parameters and related energy distribution. This problem shows the importance of microstructural parameters on the resulting macroscopic crack path. An application case is then proposed to highlight the related consequences in terms of crack coalescence kinetics.

Keywords: Fracture, Cosserat Media, internal lengths, phase field, Coalescence

1. Introduction

The prediction of material failure is a major issue in various industrial fields, especially for critical applications (e.g, aerospace and nuclear fields) where microstructural effects are increasingly included in prediction analysis. A thorough understanding of each stage of fracture processes (namely crack initiation, propagation and coalescence) provides for engineers more reliable means of designing against fracture in engineering structures and also pushes towards the development of new modeling strategies.

*julien.rethore@ec-nantes.fr

According to the Griffith theory [1], cracks propagate if the energy release rate, linked to the created surface and inter-facial energy, reaches a critical value. This framework describes propagation adequately but is insufficient to account for initiation, curvilinear crack path, branching and coalescence. Such analyses can only be carried out numerically. Several methods are developed to model crack propagation, which can be divided into two groups according to the representation of cracks: discrete, such as cohesive surfaces [2] and X-FEM [3, 4, 5] or diffuse, such as non-local approaches [6] or phase field method [7], among others.

The modeling proposed in this paper is based on the phase field method (PFM) for failure which is a versatile approach to model sharp interfaces using a continuous variable. This field interpolates between the unbroken and the broken states by smooth transitions over a characteristic distance ℓ_d [8]. This method is able to easily simulate complex cracking processes including initiation, coalescence, propagation and bifurcation [9, 10, 7]. Also, its versatility allows to incorporate both isotropic and anisotropic material behaviors [11, 12]. A unified approach of this method is also proposed to deal with interfaces [13, 14, 15].

The introduction of microstructural effects (such as grain size effect in metals [16]) can impact the failure properties of materials. This is why the present work investigates how the microstructural effects can be inserted through a formalism of generalized continua. Such media are classically classified into two classes of model [17]: (i) higher grade media introducing gradients of the displacement field or some internal variables of order greater than one and (ii) higher order media introducing additional degrees of freedom to the displacement field in the framework of the first gradient theory.

In the present work, attention is drawn to the Cosserat continuum which was first proposed in 1909 by Cosserat brothers [18]. The integral formulation of the constitutive equations of non-local media is established by Eringen [19]. In this medium, independent displacement $\underline{u}$ and microrotation $\underline{\phi}$ degrees of freedom are attributed to each material point. The Cosserat continuum model is frequently used for describing complex media such as composites[20], cellular solids [21], lattices [22], geometrically necessary dislocation in polycrystals [23, 24, 25], etc. Furthermore, Cosserat's theory has been shown to retain its ability to account for modeling scale effects in fracture phenomena [26] and in

localization problems [27].

The present contribution aims at implementing the PFM in the Cosserat continuum to implicitly account for microstructural effects in macroscopic responses. In [28], a cohesive micropolar phase field fracture theory has been proposed to deal with the dependency of the macroscopic Cosserat continua responses on the phase field regularization parameter by introducing a distinctive degradation function. In the present work, we focus on effects of microstructural length scales on cracks propagation in elastic Cosserat media with the standard phase field fracture model [10, 29, 30]. For this purpose, the phase field regularization length will be chosen smaller than the length scale introduced by the Cosserat medium. This paper will allow to highlight the non negligible effect of micro/macro interactions on crack paths and cracks coalescence.

This paper is structured as follows: in Section 2, the PFM is developed relying on the Cosserat media framework. The role of micro/macro parameters on crack path variability is analyzed in Section 3 through a simple shear problem where global energy distribution and local fields are examined. Then, in Section 4, a complex simulation of a coalescence problem [31] is performed to highlight effects of the Cosserat medium on the coalescence of cracks.

2. Methods

2.1. Cosserat media

The continuum in the Cosserat theory is characterized by a displacement field $\underline{u}$ and a microrotation field independent of each other:

$$DOF = \{\underline{u}, \underline{\phi}\}. \tag{1}$$

The Cosserat medium is a particular representation of the more general micromorphic approach [32] where the underlying triad of rigid vectors attached to the microstructure is not deduced from the continuum material point by an arbitrary transformation but by a microrotation (that can be described by a pseudo-vector $\underline{\Phi}$). In the general case, this microrotation does not coincide with the macroscopic material rotation associated with the anti-symmetric part of the transformation gradient. From these fields, the relative

deformation tensor $\underset{\sim}{e}$ and the torsion-curvature tensor $\underset{\sim}{\kappa}$ are generally not symmetric and defined by [1]:

$$\begin{aligned} \underset{\sim}{e} &= \nabla \underline{u} + \underset{\sim}{\epsilon}\underline{\phi}, \\ \underset{\sim}{\kappa} &= \nabla \underline{\phi}. \end{aligned} \tag{2}$$

where ϵ and ∇ denote the permutation tensor and the gradient operator respectively. The relative deformation between macroscopic and microscopic scales represents the difference between the displacement gradient and the microrotation.

The stress measures associated with the deformation rates are the force stress tensor $\underset{\sim}{\sigma}$ and the couple stress tensor $\underset{\sim}{M}$ which must satisfy the following balance equations:

$$\begin{aligned} div(\underset{\sim}{\sigma}) &= 0, \\ div(\underset{\sim}{M}) - \underset{\sim}{\epsilon} : \underset{\sim}{\sigma} &= 0. \end{aligned} \tag{3}$$

For the sake of simplicity, these equations are written in the static case and volume forces and couples are excluded. A more general description can be found in [19]. The associated traction vector $\underline{t}$ and the couple stress vector $\underline{m}$ acting on a surface element must fulfill the following boundary conditions:

$$\begin{aligned} \underline{t} &= \underset{\sim}{\sigma}.\underline{n}, \\ \underline{m} &= \underset{\sim}{M}.\underline{n}. \end{aligned} \tag{4}$$

where $\underline{n}$ is the outward oriented normal vector.

In the framework of linear elasticity, $(\underset{\sim}{\sigma}, \underset{\sim}{M})$ is linked to $(\underset{\sim}{e}, \underset{\sim}{\kappa})$ by a generalized Hooke law [17]:

$$\begin{aligned} \underset{\sim}{\sigma} &= \underset{\approx}{A} : \underset{\sim}{e}, \\ \underset{\sim}{M} &= \underset{\approx}{E} : \underset{\sim}{\kappa}. \end{aligned} \tag{5}$$

where $\underset{\approx}{A}(Pa)$ and $\underset{\approx}{E}(Pa.m^2)$ are the generalized elasticity tensors. For isotropic materials which is the scope of this work, the generalized Hooke law is written using six independent

[1] In this paper, $\underline{\ }$ denotes the first order tensor, $\underset{\sim}{\ }$ the second order, combination of them $\underset{\sim}{\underline{\ }}$ is used for the third order and $\underset{\approx}{\ }$ denotes the fourth order tensor.

elastic moduli:

$$\begin{aligned} \underset{\sim}{\sigma} &= \lambda tr(\underset{\sim}{e})\underset{\sim}{I} + 2\mu \underset{\sim}{e}^s + 2\mu_c \underset{\sim}{e}^a, \\ \underset{\sim}{M} &= \alpha tr(\underset{\sim}{\kappa})\underset{\sim}{I} + 2\beta \underset{\sim}{\kappa}^s + 2\gamma \underset{\sim}{\kappa}^a. \end{aligned} \tag{6}$$

Exponents ^{s} and ^{a} denote respectively the symmetric and skew-symmetric parts of the corresponding tensor. λ and μ are the Lamé coefficients. μ_c relates the skew-symmetric part of the relative deformation tensor to the skew-symmetric part of the stress tensor, α is the torsion modulus and β and γ are the bending moduli. In two-dimensions, the constant α does not intervene, and for simplicity, we generally adopt $\beta = \gamma$ as in [33]. Thus, two characteristic lengths appear when the ratio of the previous expressions in Eq. (6) is examined:

$$\ell_s = \sqrt{\frac{\beta}{\mu}}, \qquad l_a = \sqrt{\frac{\gamma}{\mu_c}} \approx \sqrt{\frac{\beta}{\mu_c}} \tag{7}$$

ℓ_s and l_a are the intrinsic length scales related respectively to the symmetric and skew-symmetric tensors of Cosserat media elasticity.

2.2. Phase field fracture in Cosserat media

In a regularized framework, the crack geometry is approximated by a damage field d such that $d = 1$ on the cracked area Γ and $d = 0$ away from it. The variational approach to fracture following [9] defines the total energy for a cracked body as:

$$\begin{aligned} E &= E_d + E_s \\ &= \int_\Omega g(d) W_d d\Omega + G_c \int_\Omega \gamma(d, \nabla d) d\Omega. \end{aligned} \tag{8}$$

In Eq. (8), E_d represents the elastic energy stored in the cracked body which can be expressed as the integral of the product of the elastic energy density and a degradation function describing the damage of the material as a function of the phase field d and is usually chosen to have the simple quadratic form [34]:

$$g(d) = (1 - d)^2. \tag{9}$$

For the Cosserat media, elastic energy density is expressed as:

$$W_{\underline{u},\underline{\Phi}}(\underset{\sim}{e}, \underset{\sim}{\kappa}) = \frac{1}{2}\underset{\sim}{e} : \underset{\approx}{A} : \underset{\sim}{e} + \frac{1}{2}\underset{\sim}{\kappa} : \underset{\approx}{E} : \underset{\sim}{\kappa}. \tag{10}$$

To avoid the issue of crack faces interpenetration under normal compression loading, the hybrid formulation proposed by Ambati *et al.* [29] is adopted in this work. This formulation keeps linear the displacement problem and the damage field evolution is only controlled by the part of elastic energy responsible for crack propagation $W^{+}_{\underset{\sim}{u},\underset{\sim}{\Phi}}$ according to Amor *et al.* [30] . Atroshchenko *et al.* [26] showed that the generalized stress intensity factors are linked to both displacement and microrotation fields. In this work, we assume that the skew-symmetric part of relative deformation, $\underset{\sim}{e}$, and the curvature tensor, $\underset{\sim}{\kappa}$, of the Cosserat medium drive the phase field evolution. The negative part of elastic energy is then defined as in Cauchy media:

$$\begin{cases} W^{-}_{\underset{\sim}{u},\underset{\sim}{\Phi}}(\underset{\sim}{e},\underset{\sim}{\kappa}) = 0 & \text{if } tr(\underset{\sim}{e}) > 0 \quad (11a) \\ W^{-}_{\underset{\sim}{u},\underset{\sim}{\Phi}}(\underset{\sim}{e},\underset{\sim}{\kappa}) = \frac{1}{2}\underset{\sim}{e} : (k_0 1 \otimes 1) : \underset{\sim}{e}, & \text{if } tr(\underset{\sim}{e}) < 0 \quad (11b) \end{cases}$$

where k_0 is the bulk modulus of the undamaged material.

In Eq. 8, E_s is the energy required to create/propagate the crack according to the Griffith criterion which is expressed as the product of the fracture energy G_c (energy required to create a unit surface crack) and the crack surface functional.

We deduce the free energy to be minimized for the phase field problem:

$$W = g(d)W^{+}_{\underset{\sim}{u},\underset{\sim}{\Phi}}(\underset{\sim}{e},\underset{\sim}{\kappa}) + W^{-}_{\underset{\sim}{u},\underset{\sim}{\Phi}}(\underset{\sim}{e},\underset{\sim}{\kappa}) + G_c\gamma(d,\nabla d). \quad (12)$$

where $\gamma(d)$ represents the crack density function per unit volume, defined by:

$$\gamma(d,\nabla d) = \frac{1}{2\ell_d}d^2 + \frac{\ell_d}{2}\nabla d.\nabla d. \quad (13)$$

Assuming isothermal processes, the Clausius-Duhem inequality is applied to derive the governing equations for the mechanical response and the phase-field evolution:

$$\underset{\sim}{\sigma} : \underset{\sim}{\dot{e}} + \underset{\sim}{M} : \underset{\sim}{\dot{\kappa}} - \dot{W} \geq 0. \quad (14)$$

After development of Eq. (14), one obtains:

$$-\frac{\partial W}{\partial d}.\dot{d} \geq 0. \quad (15)$$

and by substituting Eq. (12) in Eq. (15):

$$2(1-d)W^{+}_{\underset{\sim}{u},\underset{\sim}{\Phi}}(\underset{\sim}{e},\underset{\sim}{\kappa}) - \frac{G_c}{\ell_d}(d - l_d^2\Delta d) = 0 \quad if \quad \dot{d} > 0. \quad (16)$$

In order to deal with the loading and unloading history and to ensure the positiveness of $\dot{d}$ even for unloading conditions, we follow Miehe's proposal [10] by replacing $W^+_{\underset{\sim}{u},\underline{\Phi}}(\underset{\sim}{e},\underset{\sim}{\kappa})$ in Eq. (16) by a history function:

$$\mathcal{H}(\underline{x},t) = \underset{\tau\in[0,t]}{max}\{W^+_{\underset{\sim}{u},\underline{\Phi}}(\underline{u}(\underline{x},\tau),\underline{\Phi}(\underline{x},\tau))\} \quad \forall \quad \underline{x}\in\Omega. \tag{17}$$

A threshold $\phi_c = \frac{G_c}{2\ell_d}$ is added to the history function Eq. (17) to prevent numerical damage at low stress levels [35]:

$$\mathcal{H}(\underline{x},t) = \underset{\tau\in[0,t]}{max}\{\underset{\tau\in[0,t]}{max}\{W^+_{\underset{\sim}{u},\underline{\Phi}}(\underline{u}(\underline{x},\tau),\underline{\Phi}(\underline{x},\tau))\} - \phi_c, 0\} \quad \forall \quad \underline{x}\in\Omega. \tag{18}$$

Then, the phase field problem to be solved to evaluate $d(\underline{x},t)$ at time t is:

$$\begin{cases} 2(1-d)\mathcal{H} - \dfrac{G_c}{\ell_d}(d - l_d^2\Delta d) = 0 \quad in \quad \Omega, & (19a)\\ d(\underline{x}) = 1 \quad on \quad \Gamma, & (19b)\\ \nabla d(\underline{x}).\underline{n} = 0 \quad on \quad \partial\Omega. & (19c) \end{cases}$$

In the framework of the hybrid decomposition, the phase field problem to be solved in Cosserat media is then:

$$\begin{cases} \mathcal{H}(\underline{x},t) = \underset{\tau\in[0,t]}{max}\{W^+_{\underset{\sim}{u},\underline{\Phi}}(\underline{u}(\underline{x},\tau),\underline{\Phi}(\underline{x},\tau))\}, & (20a)\\ 2(1-d)\mathcal{H} - \dfrac{G_c}{\ell_d}(d - l_d^2\Delta d) = 0, & (20b) \end{cases}$$

and the displacement problem is:

$$\begin{cases} \forall \underline{x}: \quad \text{if} \quad W^+_{\underset{\sim}{u},\underline{\Phi}} < W^-_{\underset{\sim}{u},\underline{\Phi}} \quad \text{then} \quad d = 0, & (21a)\\ \underset{\sim}{\sigma} = \dfrac{\partial W(\underset{\sim}{e},\underset{\sim}{\kappa},d)}{\partial \underset{\sim}{e}} = (1-d)^2\dfrac{\partial W_{\underset{\sim}{u}}(\underset{\sim}{e})}{\partial \underset{\sim}{e}}, & (21b)\\ \underset{\sim}{M} = \dfrac{\partial W(\underset{\sim}{e},\underset{\sim}{\kappa},d)}{\partial \underset{\sim}{\kappa}} = (1-d)^2\dfrac{\partial W_{\underline{\Phi}}(\underset{\sim}{\kappa})}{\partial \underset{\sim}{\kappa}}. & (21c) \end{cases}$$

In practice, as in e.g. [15], a small parameter k is introduced in Eq. (21b) and Eq. (21c), chosen as small as possible to maintain the well-posedness of the problem.

3. Model Analysis

To investigate effects of Cosserat media on crack paths, we will study a phase field benchmark problem [7] which highlights the effects of length scales on cracking mecha-

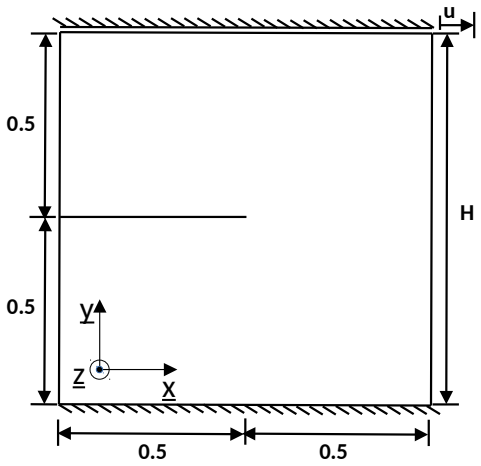

Figure 1: Geometry and boundary conditions of single-edge notched shear test, top and bottom edges Cosserat microrotation are fixed

nisms. The classical benchmark problem is a single-edge notched shear test that consists of a square with a horizontal notch. The geometrical setup and the boundary conditions are depicted in Fig. 1. We use a relatively fine uniform mesh with 20100 first order triangular elements. The displacement is prescribed along the $x-$direction for the upper edge while the displacement along y and microrotation around z are fixed. Displacement increments are fixed as $\Delta u = 1 \times 10^{-5}$ mm throughout the loading history. Along the bottom edge, all the displacements and the microrotation are fixed.

The material parameters are the same as in [7, 29] for the classical Lamé's constants:

$$\lambda = 121.15GPa, \quad \mu = 80.77GPa \tag{22}$$

and the phase field parameters are:

$$G_c = 2700J/m^2, \quad \ell_d = 2 \times 10^{-5}m \tag{23}$$

All the cases in the present work are in 2D under plane strain assumption. To compare the simulation results, we define R_s and R_a as the ratios between the characteristic lengths ℓ_s and l_a, respectively, and the size of the square specimen H:

$$R_s = \frac{\ell_s}{H}, \quad R_a = \frac{l_a}{H}. \tag{24}$$

Then, to understand the contributions of each of the internal energies, the following decomposition is proposed:

- Symmetric part: $W_{\underset{\sim}{u}}(\underset{\sim}{e}^s) = \frac{1}{2}\underset{\sim}{\sigma}^s : \underset{\sim}{e}^s$
- Skew-Symmetric part: $W_{\underset{\sim}{u}}(\underset{\sim}{e}^a) = \frac{1}{2}\underset{\sim}{\sigma}^a : \underset{\sim}{e}^a$
- Curvature part: $W_{\underset{\sim}{\Phi}}(\underset{\sim}{\kappa}) = \frac{1}{2}\underset{\sim}{M} : \underset{\sim}{\kappa}$

These energies will be normalized by the total dissipated energy for each case so that the energy variations can be compared in a quantitative way.

According to the results of Miehe *et al.* [7], the phase field regularization parameter ℓ_d should always be taken at least two times larger than the smallest element size. All simulations are performed in the finite element code Cast3M [36] where we developed the Cosserat media and implemented the proposed PFM.

3.1. Global parametric study

To assess effects of Cosserat media on the crack patterns, a parametric study is performed by varying the Cosserat additional parameters μ_c and β. The initial values of these parameters are chosen as:

- $\mu_{cI} = \mu$ as μ_c should be greater or equal to μ.
- $\beta_I = 132$ Pa.m^2 to ensure that for the initial value of μ_c, $\ell_s > \ell_d$.

and they will vary between $[1, 100] \times \mu$ and $[1, 100] \times \beta_I$ respectively.

For each simulation: i) the maximum variation of the energies $W_{\underset{\sim}{u}}(\underset{\sim}{e}^s)$, $W_{\underset{\sim}{u}}(\underset{\sim}{e}^a)$ and $W_{\underset{\sim}{\Phi}}(\underset{\sim}{\kappa})$ in time and ii) the height of the crack at 75% of its propagation along the x-direction will be saved and used for Fig. 3. 75% of x-direction was chosen to avoid boundary effects that would have affected the crack path when it reaches the edges.

Fig. 2 provides the energy maps and Fig. 3 the crack heights at the relevant x position. These figures highlight the nonlinear dependency of these quantities with respect to Cosserat parameters. Fig. 2c shows that the skew-symmetric energy is affected by the variation of β at low values of μ_c. When μ_c takes higher values, the contribution of this energy becomes negligible. This is consistent with Forest's works [37] which assumes that μ_c is a penalty factor that constrains the Cosserat directors to be the lattice vectors.

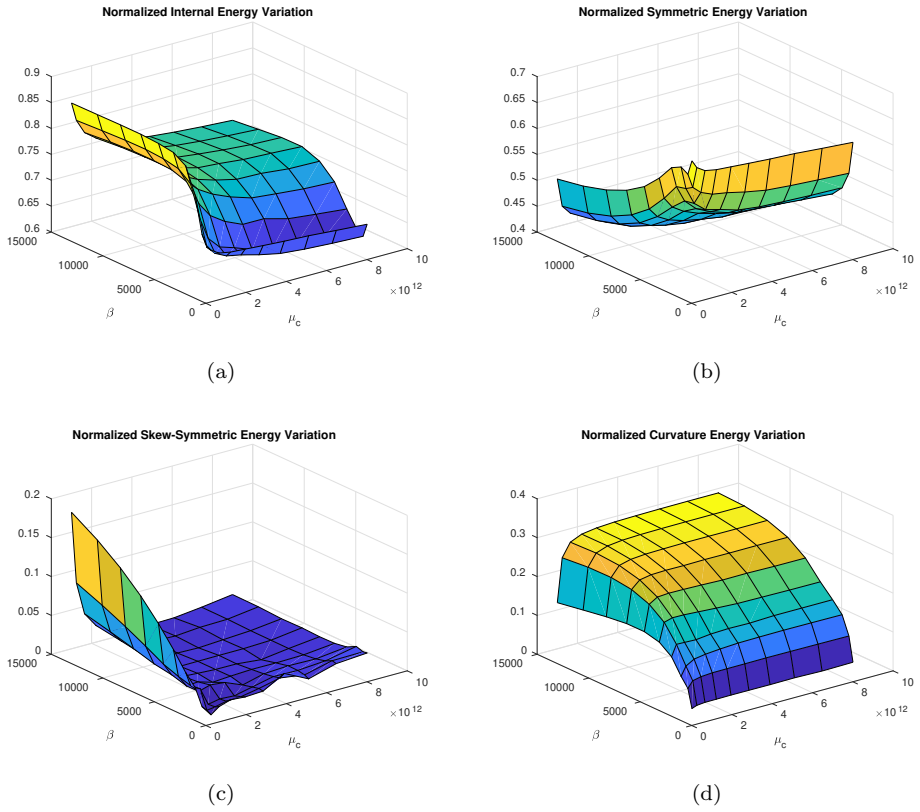

Figure 2: Single-edge notched shear test. 3D maps of energy decomposition for different Cosserat parameters: (a)Normalized internal energy, (b)Normalized Symmetric energy, (c)Normalized Skew-Symmetric energy, (d)Normalized Curvature energy.

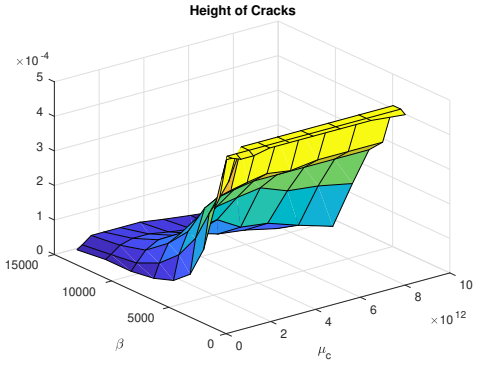

Figure 3: Single-edge notched shear test. Height of cracks map for different Cosserat parameters.

The curvature energy (Fig. 2d) is affected by the parameter β but not by μ_c, as β is the bending modulus. As β increases, the curvature energy increases and thus, the curvature of crystal lattice is penalized (Fig. 3).

The effect of Cosserat parameters on crack deflection can be seen in Fig. 3. For low values of β, height of cracks increases when μ_c increases. However, when β is high, μ_c is no longer able to make the Cosserat directors converge to the lattice vectors, which is consistent with the energetic analysis.

This parametric study allows to have a global vision about the effects of Cosserat parameters on energy distributions and crack paths. To provide more insight on these length scales effects we decided to:

- provide a deeper analysis by following crack path and energy evolution as function of prescribed displacements.
- analyze the local fields in order to determine if the crack deflections are influenced by the global effects mentioned above or the local fields.
- analyze the two previous items through (i) a first series of simulations where both ℓ_s and l_a are varying in a similar manner (setting $\mu = \mu_c$) by varying the parameter β, (ii) and a second series for which l_s is fixed and l_a is varying (β is prescribed and μ_c is modified).

3.2. Varying β with $l_s = l_a$

In this subsection, we will analyze results from the previous global study related to the variation of Cosserat intrinsic lengths l_s and l_a by taking $\mu = \mu_c$ and varying the parameter β such as $R = R_s = R_a$. Four tests are proposed following this guideline:

- $\beta = 132$ Pa.m^2 $\Longrightarrow \ell_s = \ell_a = 4 \times 10^{-5}$ m$\Longrightarrow R = 0.04$,
- $\beta = 528$ Pa.m^2 $\Longrightarrow \ell_s = \ell_a = 8 \times 10^{-5}$ m$\Longrightarrow R = 0.08$,
- $\beta = 2112$ Pa.m^2 $\Longrightarrow \ell_s = \ell_a = 16 \times 10^{-5}$ m$\Longrightarrow R = 0.16$,
- $\beta = 8448$ Pa.m^2 $\Longrightarrow \ell_s = \ell_a = 32 \times 10^{-5}$ m$\Longrightarrow R = 0.32$.

For these four cases, the crack patterns and load–displacement curves are shown in Fig. 4 and Fig. 5 and compared to the results obtained for a classical Cauchy medium. It is clear that the crack patterns are highly influenced by the Cosserat parameters when the microstructural scale exceeds 8% of the structure scale. The higher the R is, the lesser is the curvature in the crack trajectory and the higher is the force needed to initiate the crack is. To understand the contribution of these parameters on crack patterns, the energy decomposition evolution in time is presented in Fig. 6:

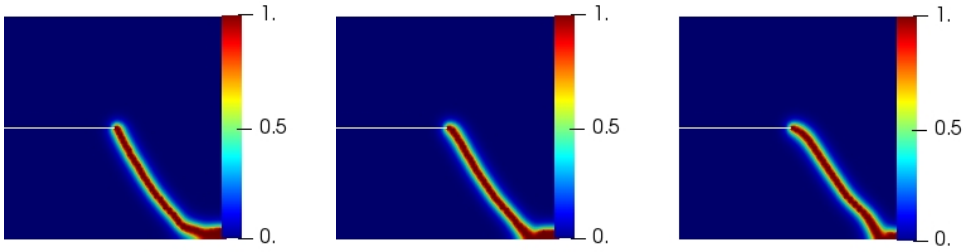

(a) Cauchy media (b) $R = 0.04$ (c) $R = 0.08$

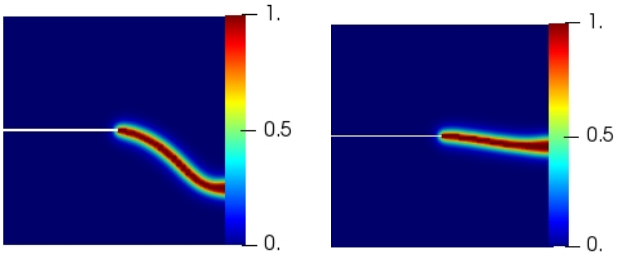

(d) $R = 0.16$ (e) $R = 0.32$

Figure 4: Single-edge notched shear test. Crack patterns in a Cauchy medium (a) and Cosserat media for different R (b-e).

As expected, Fig. 6 shows that the curvature energy increases with β. We can also notice that even if μ_c is fixed the skew part of the energy increases sharply (cf. Fig. 6c) as R increases. This point suggests that, at the structural scale, the relative rotation between the non symmetric part of displacement gradient and the Cosserat microrotation

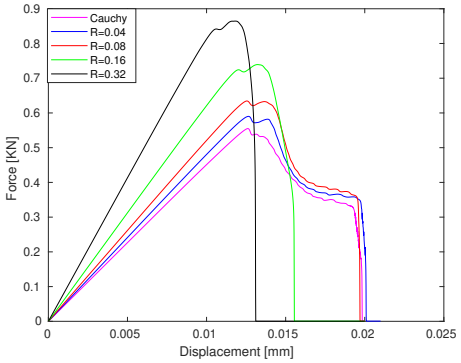

Figure 5: Single-edge notched shear test. Load–displacement curves in a Cauchy medium and Cosserat media for different R.

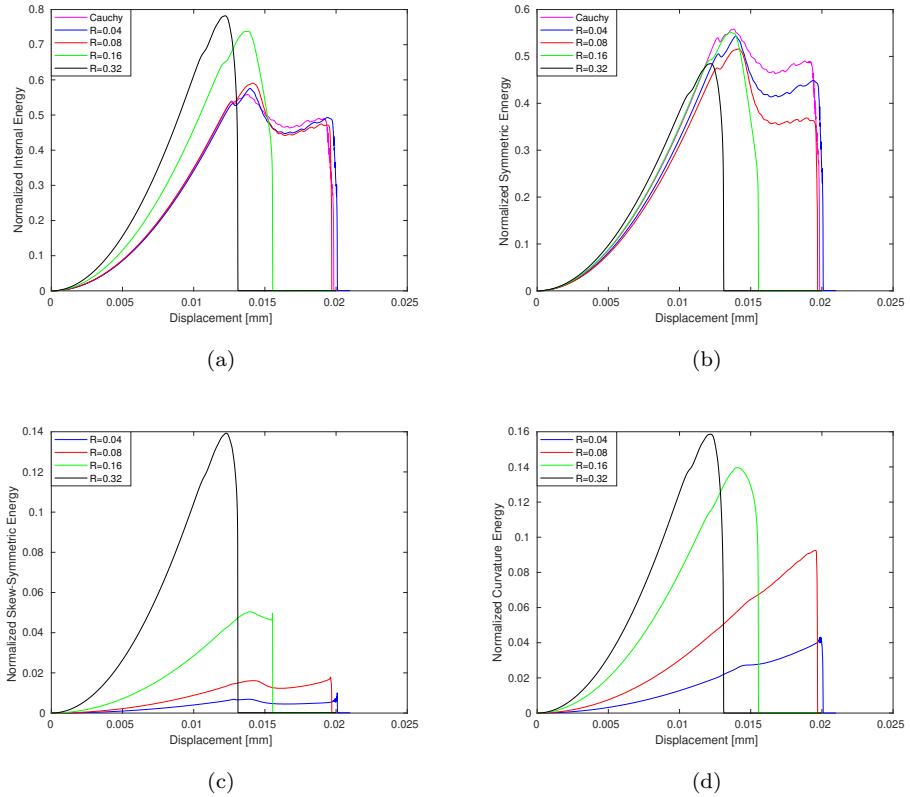

Figure 6: Single-edge notched shear test. Comparison of the energy decomposition for a Cauchy medium and Cosserat media with different R: (a)Normalized internal energy, (b)Normalized Symmetric energy, (c)Normalized Skew-Symmetric energy, (d)Normalized Curvature energy.

is large. For all simulations, it is difficult to predict the beginning of the deflection of cracks from the evolution of energies. Also, one can notice that both of the Cosserat effects are active at the very beginning of simulations and could affect crack path at initiation.

To go further in the analysis, micro and macro rotations maps are presented in Fig. 7. From the analysis of these maps, when R is larger (resulting in a larger β and curvature energy), the microrotation gradient is penalized (Fig. 7b-7d) and the field becomes more diffused. This dominates over the effect of macrorotation on the crack patterns, as shown in Fig. 7f-7h, resulting in cracks converging to horizontal paths. The crack path follows the one obtained with a Cauchy model when strong microrotation gradients (Fig. 7a) are produced ahead of the crack tip.

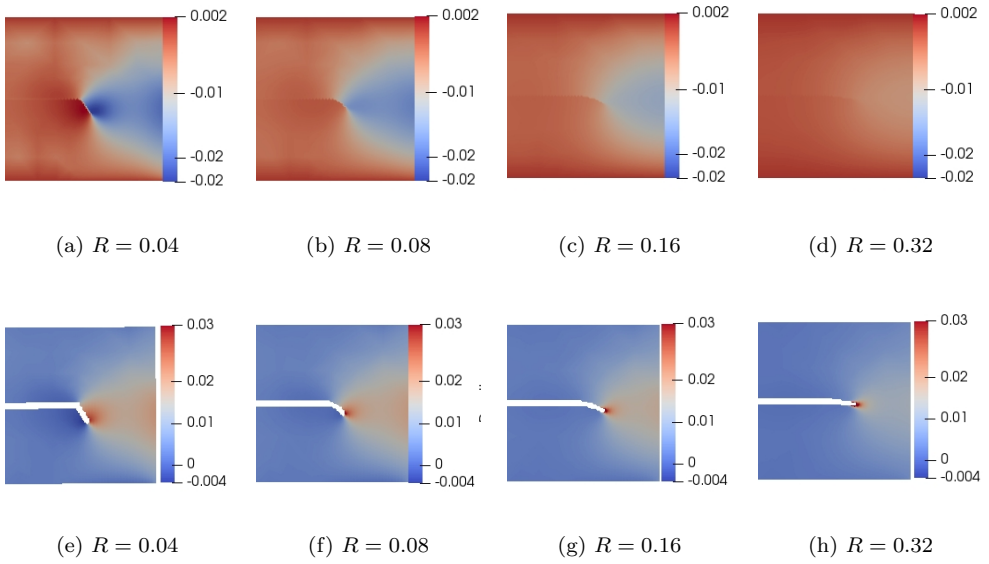

(a) $R = 0.04$ (b) $R = 0.08$ (c) $R = 0.16$ (d) $R = 0.32$

(e) $R = 0.04$ (f) $R = 0.08$ (g) $R = 0.16$ (h) $R = 0.32$

Figure 7: Single-edge notched shear test. Cosserat microrotations (a-d) and macrorotation (e-h) after crack initiation for different R.

3.3. Fixing l_s and varying l_a

In this second specific study, to highlight the effects of the skew-symmetric part, ℓ_s is fixed and ℓ_a will be varied via the parameter μ_c. ℓ_s is chosen equal to 16×10^{-5} m since

the Cosserat medium already shows, in the previous paragraph, that crack deflection can be produced. Then, four simulations are performed:

- $\mu_c = \mu \Longrightarrow \ell_a = 8 \times 10^{-5}$ m$\Longrightarrow R_a = 0.08$,
- $\mu_c = 5\mu \Longrightarrow \ell_a = 5 \times 10^{-5}$ m$\Longrightarrow R_a = 0.03$,
- $\mu_c = 20\mu \Longrightarrow \ell_a = 1.8 \times 10^{-5}$ m$\Longrightarrow R_a = 0.018$,
- $\mu_c = 40\mu \Longrightarrow \ell_a = 1.2 \times 10^{-5}$ m$\Longrightarrow R_a = 0.012$.

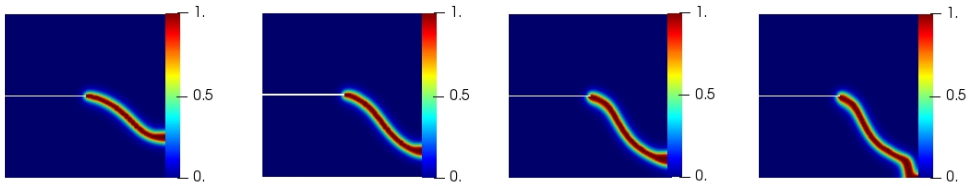

(a) $R_a = 0.08$ (b) $R_a = 0.03$ (c) $R_a = 0.018$ (d) $R_a = 0.012$

Figure 8: Single-edge notched shear test. Crack patterns in Cosserat media for different R_a with $R_s = 0.16$.

The crack patterns and load–displacement curves are shown in Fig. 8 and Fig. 9. We notice that the smaller the R_a is, (i) the more curved the crack trajectory is (convergence to the Cauchy medium response), (ii) and the higher the material toughness is Fig. 9. In this case, as presented in Fig. 10d, the curvature energy is not significantly affected, contrary to the skew symetric part Fig. 10c. We can thus suggest that the energy related to the skew symmetric part is sufficient to deviate the crack. Again, energetic contribution is not predictive of crack deflection kinetics. Therefore, an analysis of the local fields is carried out.

The related micro and macro rotations maps are presented in Fig. 11. When R_a is small (μ_c is large), the relative rotation is penalized, then i) the microrotation follows the macrorotation, ii) the skew-symmetric energy part is reduced (Fig. 10c) and iii) the curvature energy is slightly higher (Fig. 10d). In this case, the effects of macrorotation dominate and control the crack pattern (Fig. 11e-11h). The microrotation field (Fig. 11a) is diffuse at the beginning and becomes more and more intense when Cosserat

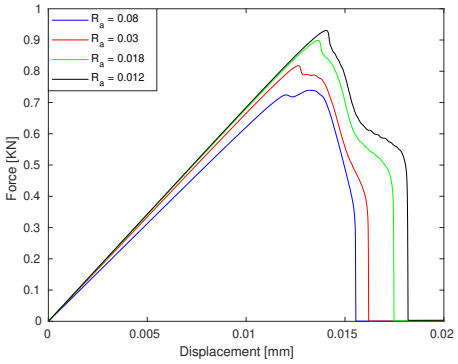

Figure 9: Single-edge notched shear test. Load–displacement curves in Cosserat media for different R_a with $R_s = 0.16$.

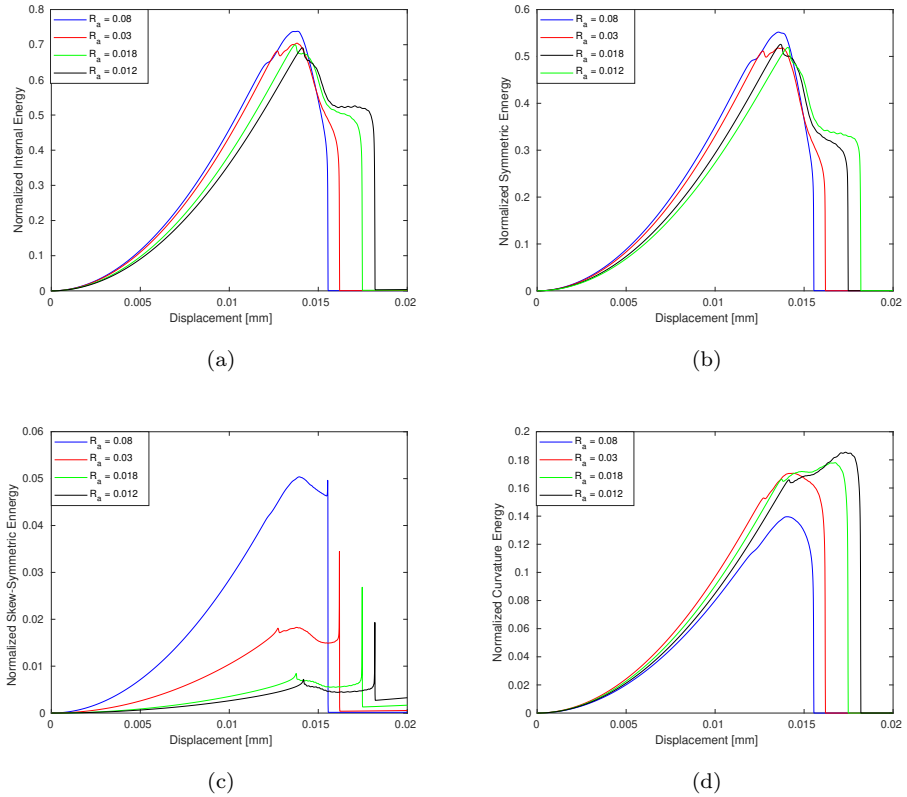

Figure 10: Single-edge notched shear test. Comparison of the energy decomposition for different R_a of the Cosserat medium: (a) Normalized internal energy, (b) Normalized Symmetric energy, (c) Normalized Skew-Symmetric energy, (d) Normalized Curvature energy.

stiffness increases (here μ_c). Here again, the crack path follows what is predicted with Cauchy framework when strong microrotation gradients are produced ahead of the crack tip.

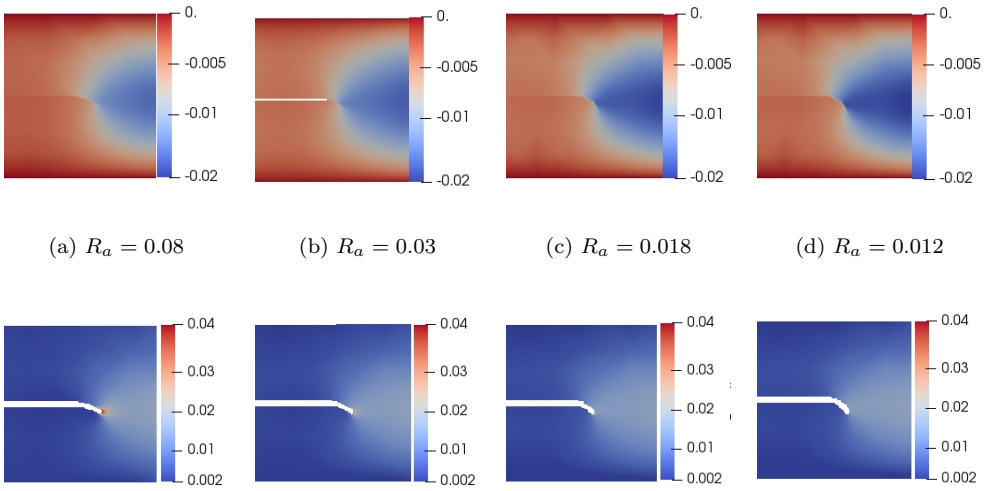

(a) $R_a = 0.08$ (b) $R_a = 0.03$ (c) $R_a = 0.018$ (d) $R_a = 0.012$

(e) $R_a = 0.08$ (f) $R_a = 0.03$ (g) $R_a = 0.018$ (h) $R_a = 0.012$

Figure 11: Single-edge notched shear test. Cosserat microrotations (a-d) and macrorotation (e-h) after crack initiation for different R_a.

3.4. Synthesis

This benchmark problem allowed us to bring to the forefront the effect of the Cosserat medium on the fracture mechanisms. Variation of the Cosserat parameters change i) the fracture path, ii) the energy distribution, iii) the local rotation fields and iv) the material toughness. The global parametric study in 3.1 has shown variation of the maximum of energies partition and the fracture paths. Despite the large effects of the parameters β and μ_c , it is difficult to correlate crack path deflection with the evolution of macroscopic energy distribution. To provide more explanations about these macroscopic results, the effects of Cosserat intrinsic lengths are discussed through a local analysis of crack paths related to macro and microrotation fields.

As the shear (horizontal) displacement is prescribed to the structure, a strong rotational macroscopic gradient is produced ahead of the crack tip due to the separation

between the top and bottom parts of the model. This rotation field produces a similar microrotation field in the structure through μ_c rigidity. When the two intrinsic lengths of the Cosserat media increase (μ_c fixed and β increases), the crystal curvature is penalized. As a result, the Cosserat microrotation is smeared over the distance ℓ_s. Consequently, to avoid extensive curvature energy ahead of crack tip, the crack propagates in the horizontal direction. This occurs when the microstructural scales (ℓ_s and ℓ_a) exceed 8% of the structure scale.

In the other hand, reducing the intrinsic length ℓ_a (by increasing μ_c) relative to the skew-symmetric part of the medium allows microrotation gradient to follow the macrorotation gradient. This leads to crack trajectories converging towards those obtained with a Cauchy medium. It should be noted that this effect of ℓ_a on the crack trajectory is valid only for low values of β. When the microstructural scale exceeds 16% of the structure scale, $R_s > 0.16$, the effect of β dominates over that of μ_c. The curvature (microrotation gradient) becomes sufficiently smooth to drive the crack in the horizontal direction in order to prevent a high local energy concentration ahead of the crack tip.

4. Application: coalescence test

To highlight the effect of the Cosserat medium on crack path prediction in a practical application, an asymmetric double notched tensile problem, inspired from [38] is chosen. The geometrical setup and the boundary conditions are depicted in Fig. 12 as in [39]. The material properties are the same as in the previous example 3 and the PFM parameters are:

$$G_c = 2700 J/m^2, \quad \ell_d = 0.2 \times 10^{-3} m. \tag{25}$$

The mesh is refined around the expected cracking zone, with the size of 0.1 mm which seems to be enough to eliminate the mesh-related effects. The displacement is prescribed along the y-direction for the upper edge while the displacement along x and the microrotation around z are free. The displacement control is used with increments $\Delta u = 1 \times 10^{-4}$ mm for 400 steps, then $\Delta u = 1 \times 10^{-5}$ mm for the rest of the simulation to precisely follow the evolving fracture patterns. Fig. 13a shows the fracture pattern in the Cauchy medium where cracks do not coalesce. In the Cosserat medium, we will vary

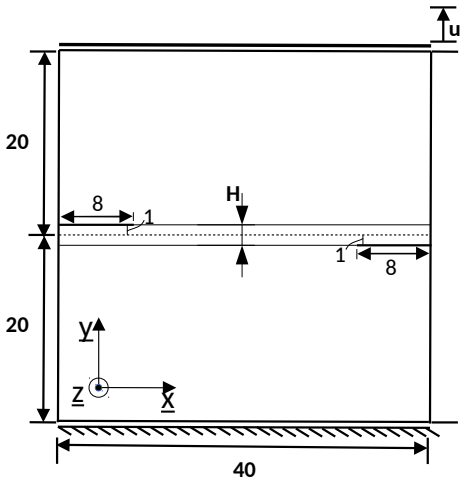

Figure 12: Geometry and boundary conditions for the asymmetric double notched tensile test

both ℓ_s and ℓ_a by setting $\mu_c = \mu$ and varying β to show the variation of the fracture pattern. For this purpose, four cases are studied:

- $\beta = 240 \times 10^3$ Pa.m^2 $\Longrightarrow \ell_s = 1.72 \times 10^{-3}$ m$\Longrightarrow R = 0.86$,
- $\beta = 960 \times 10^3$ Pa.m^2 $\Longrightarrow \ell_s = 3.44 \times 10^{-3}$ m$\Longrightarrow R = 1.72$,
- $\beta = 3840 \times 10^3$ Pa.m^2 $\Longrightarrow \ell_s = 6.89 \times 10^{-3}$ m$\Longrightarrow R = 3.44$.
- $\beta = 15360 \times 10^3$ Pa.m^2 $\Longrightarrow \ell_s = 10.37 \times 10^{-3}$ m$\Longrightarrow R = 5.18$,

where $R = R_s = R_a$ is defined as in Eq. (24) with H the vertical distance between the pre-cracks which is the relevant structural length scale of this problem.

Fig. 13 shows the fracture patterns depending on the Cosserat parameters. One can notice that the intrinsic lengths of the Cosserat medium control the interactions between cracks. The larger these lengths are, the faster the cracks merge. For $R = 1.72$, the fracture path is roughly similar to the one in the Cauchy medium. When R reaches 3.44, the two cracks come close to each other but they don't coalesce. Simulations from $R = 6.89$ (internal length much higher than structural length) show that the coalescence of carcks occurs. To understand the governing mechanisms behind these results, the induced variation on the maps of the Cosserat microrotation and the macrorotation are examined (Fig. 14).

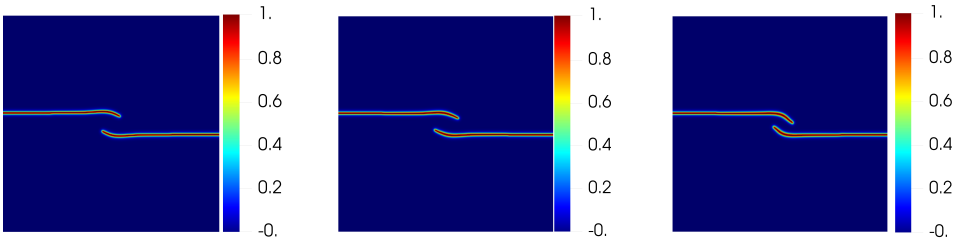

(a) Cauchy media (b) $R_s = 1.72$ (c) $R_s = 3.44$

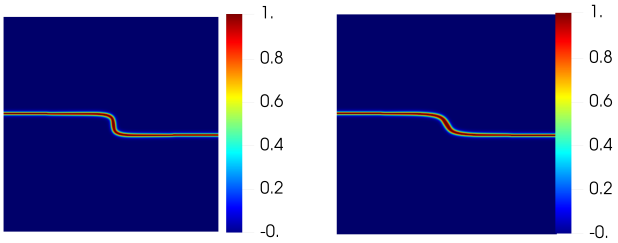

(d) $R_s = 6.89$ (e) $R_s = 10.37$

Figure 13: Asymmetric double notched tensile specimen. Crack patterns in a Cauchy medium (a) and Cosserat media for different R (b-e).

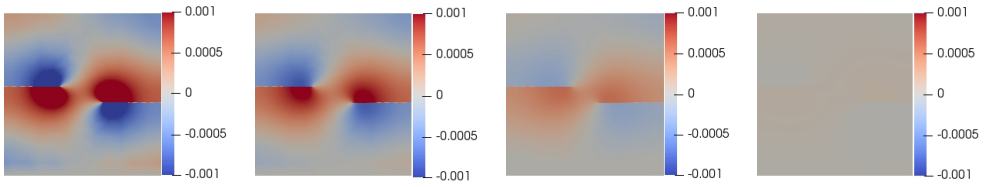

(a) $R = 1.72$ (b) $R = 3.44$ (c) $R = 6.89$ (d) $R = 10.37$

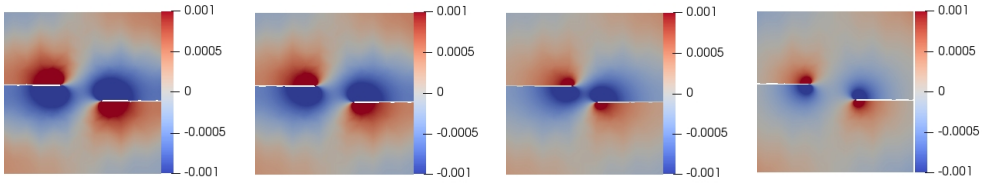

(e) $R = 1.72$ (f) $R = 3.44$ (g) $R = 6.89$ (h) $R = 10.37$

Figure 14: Asymmetric double notched tensile specimen. Cosserat microrotations (a-d) and macrorotations (e-h) after crack initiation for different R.

The rotation maps in Fig. 14 show that the gradient of macrorotation induced by the applied boundary conditions is strong close to the crack tips (Fig. 14e). The corresponding gradient of microrotation follows similar variation (Fig. 14a). For low length scale (low β), the microrotation gradient is not so penalized such that the cracks can go horizontally and they interact through their microrotation gradient. However when β is high (large length scale), the microrotation gradient is reduced. The model produces such gradient reduction by inducing more diffuse fields and by following the shortest crack path to compensate left and right gradients associated to the crack tips. This coalescence test emphasizes effects of the Cosserat medium on the crack paths. It demonstrates the importance of taking into account the scale effects on crack fracture mechanisms.

5. Conclusion

In this paper, a new approach for modeling different fracture mechanisms is proposed through the influence of internal lengths effects on crack patterns at the macroscopic scale. The PFM was chosen to model complex cracking processes in an efficient manner.

This method was coupled to the Cosserat media which allows to model microstructural size effects (e.g, geometrically necessary dislocations) while keeping intact the singularity of the stress field at the crack tip. In these developments the effect of the two intrinsic lengths of the Cosserat media was highlighted by studying their effect on single crack propagation and coalescence phenomena. The internal energy in the Cosserat media was decomposed into a symmetric part, a skew-symmetric part and a curvature part. This decomposition makes it easier to quantify and qualify the contribution of each microstructural parameter on the macroscopic response.

However, parametric studies conducted on the single-edge notched shear test showed that the local behavior ahead of the crack tip is a better indicator to understand crack path deflection. It was shown that crack tip induces large macro and microrotation gradients for displacement controlled experiments. For a constant μ_c, it was shown that, if the microrotation gradients require high energy, the rotation field becomes more and more diffuse as the internal length increases and a deflection can be produced in order to follow the path that minimizes crystal curvature.

Then, a numerical study on a more complex case was also performed in order to highlight the impact of such effects on multi-cracked solids. The proposed model was used to highlight the strong effect of the microstructure on the coalescence occurrence and its kinetics: the more difficult the crystal curvature is, the faster the coalescence is.

The results shown in this paper manifest the importance of taking into account the size effects in the fracture mechanisms, especially in critical applications, where the development of multiple cracks can be an important part of components service life [40, 35].

Future developments might regard fracture mechanisms at the polycrystal scale, where size effects should be identified to microstructural features.

References

[1] A. Griffith, The Phenomena of Rupture and Flow in Solids, Philosophical Transactions of the Royal Society of London (1921).
URL https://royalsocietypublishing.org/doi/pdf/10.1098/rsta.1921.0006

[2] F. Zhou, J. F. Molinari, Dynamic crack propagation with cohesive elements: a methodology to address mesh dependency, International Journal for Numerical Methods in Engineering 59 (1)

(2004) 1–24. doi:10.1002/nme.857.
URL http://doi.wiley.com/10.1002/nme.857

[3] N. Moës, J. Dolbow, T. Belytschko, A finite element method for crack growth without remeshing, International Journal for Numerical Methods in Engineering 46 (1) (1999) 131–150. doi:10.1002/(SICI)1097-0207(19990910)46:1<131::AID-NME726>3.0.CO;2-J.
URL http://doi.wiley.com/10.1002/%28SICI%291097-0207%2819990910%2946%3A1%3C131%3A%3AAID-NME726%3E3.0.CO%3B2-J

[4] N. Moës, A. Gravouil, T. Belytschko, Non-planar 3D crack growth by the extended finite element and level sets-Part I: Mechanical model: NON-PLANAR 3D CRACK GROWTH-PART I, International Journal for Numerical Methods in Engineering 53 (11) (2002) 2549–2568. doi:10.1002/nme.429.
URL http://doi.wiley.com/10.1002/nme.429

[5] L. Zhao, D. Nelias, D. Bardel, A. Maynadier, P. Chaudet, B. Marie, On the fracture of multicrystalline silicon wafer, Journal of Physics D: Applied Physics 49 (47) (2016) 475601. doi:10.1088/0022-3727/49/47/475601.
URL https://iopscience.iop.org/article/10.1088/0022-3727/49/47/475601

[6] V. Lyakhovsky, Y. Hamiel, Y. Ben-Zion, A non-local visco-elastic damage model and dynamic fracturing, Journal of the Mechanics and Physics of Solids 59 (9) (2011) 1752–1776. doi:10.1016/j.jmps.2011.05.016.
URL https://linkinghub.elsevier.com/retrieve/pii/S0022509611001256

[7] C. Miehe, F. Welschinger, M. Hofacker, Thermodynamically consistent phase-field models of fracture: Variational principles and multi-field FE implementations, International Journal for Numerical Methods in Engineering 83 (10) (2010) 1273–1311. doi:10.1002/nme.2861.
URL http://doi.wiley.com/10.1002/nme.2861

[8] B. Bourdin, G. Francfort, J.-J. Marigo, Numerical experiments in revisited brittle fracture, Journal of the Mechanics and Physics of Solids 48 (4) (2000) 797–826. doi:10.1016/S0022-5096(99)00028-9.
URL http://linkinghub.elsevier.com/retrieve/pii/S0022509699000289

[9] B. Bourdin, G. A. Francfort, J.-J. Marigo, The Variational Approach to Fracture, Journal of Elasticity 91 (1-3) (2008) 5–148. doi:10.1007/s10659-007-9107-3.
URL http://link.springer.com/10.1007/s10659-007-9107-3

[10] C. Miehe, M. Hofacker, F. Welschinger, A phase field model for rate-independent crack propagation: Robust algorithmic implementation based on operator splits, Computer Methods in Applied Mechanics and Engineering 199 (45-48) (2010) 2765–2778. doi:10.1016/j.cma.2010.04.011.
URL https://linkinghub.elsevier.com/retrieve/pii/S0045782510001283

[11] T. Nguyen, J. Yvonnet, Q.-Z. Zhu, M. Bornert, C. Chateau, A phase-field method for computational modeling of interfacial damage interacting with crack propagation in realistic microstructures obtained by microtomography, Computer Methods in Applied Mechanics and Engineering 312 (2016) 567–595. doi:10.1016/j.cma.2015.10.007.

URL https://linkinghub.elsevier.com/retrieve/pii/S0045782515003266

[12] M. Paggi, J. Reinoso, Revisiting the problem of a crack impinging on an interface:A modeling framework for the interaction between the phase field approach for brittle fracture and the interface cohesive zone model, Computer Methods in Applied Mechanics and Engineering 321 (2017) 145–172. doi:10.1016/j.cma.2017.04.004.
URL https://linkinghub.elsevier.com/retrieve/pii/S0045782516317066

[13] A. C. Hansen-Dörr, M. Gude, R. Böhm, M. Kästner, Phase-field modelling of fracture in heterogeneous materials, PAMM 18 (1) (Dec. 2018). doi:10.1002/pamm.201800082.
URL https://onlinelibrary.wiley.com/doi/abs/10.1002/pamm.201800082

[14] A. C. Hansen-Dörr, R. de Borst, P. Hennig, M. Kästner, Phase-field modelling of interface failure in brittle materials, Computer Methods in Applied Mechanics and Engineering 346 (2019) 25–42. doi:10.1016/j.cma.2018.11.020.
URL https://linkinghub.elsevier.com/retrieve/pii/S0045782518305772

[15] S. Riad, D. Bardel, J. Réthoré, Unified phase field model to simulate both intergranular and transgranular failure in polycrystalline aggregates, Finite Elements in Analysis and Design 194 (2021) 103555. doi:10.1016/j.finel.2021.103555.
URL https://linkinghub.elsevier.com/retrieve/pii/S0168874X21000391

[16] U. Roy, M. Zhou, A computational framework for predicting the fracture toughness of metals as function of microstructure, Journal of the Mechanics and Physics of Solids 142 (2020) 103955. doi:10.1016/j.jmps.2020.103955.
URL https://linkinghub.elsevier.com/retrieve/pii/S0022509620301903

[17] D. P. Gianpietro, S. Pierre, F. Samuel, Mécanique des milieux continus généralisés, 2017.
URL https://www.cepadues.com/livres/mecanique-des-milieux-continus-generalises-9782364936096.html

[18] E. Cosserat, F. Cosserat, Théorie des corps déformables, 1909.

[19] A. C. Eringen, C. B. Kafadar, Polar Field Theories, in: Continuum Physics, Elsevier, 1976, pp. 1–73. doi:10.1016/B978-0-12-240804-5.50007-5.
URL https://linkinghub.elsevier.com/retrieve/pii/B9780122408045500075

[20] M. Rubin, Y. Benveniste, A Cosserat shell model for interphases in elastic media, Journal of the Mechanics and Physics of Solids 52 (5) (2004) 1023–1052. doi:10.1016/j.jmps.2003.09.030.
URL https://linkinghub.elsevier.com/retrieve/pii/S0022509603001650

[21] P. R. Onck, Cosserat modeling of cellular solids, Comptes Rendus Mécanique 330 (11) (2002) 717–722. doi:10.1016/S1631-0721(02)01529-2.
URL https://linkinghub.elsevier.com/retrieve/pii/S1631072102015292

[22] Z. Rueger, C. S. Ha, R. S. Lakes, Cosserat elastic lattices, Meccanica 54 (13) (2019) 1983–1999. doi:10.1007/s11012-019-00968-7.
URL http://link.springer.com/10.1007/s11012-019-00968-7

[23] F. NYEt, SOME GEOMETRICAL RELATIONS IN DISLOCATED CRYSTALS 10.

[24] E. Kröner, On the physical reality of torque stresses in continuum mechanics, International Journal

of Engineering Science 1 (2) (1963) 261–278. doi:10.1016/0020-7225(63)90037-5.
URL https://www.sciencedirect.com/science/article/pii/0020722563900375

[25] S. Forest, F. Barbe, G. Cailletaud, Cosserat modelling of size effects in the mechanical behaviour of polycrystals and multi-phase materials, International Journal of Solids and Structures (2000) 22.

[26] E. Atroshchenko, S. P. A. Bordas, Fundamental solutions and dual boundary element methods for fracture in plane Cosserat elasticity, Proceedings of the Royal Society A: Mathematical, Physical and Engineering Sciences 471 (2179) (2015) 20150216. doi:10.1098/rspa.2015.0216.
URL https://royalsocietypublishing.org/doi/10.1098/rspa.2015.0216

[27] H. Tang, Y. Dong, T. Wang, Y. Dong, Simulation of strain localization with discrete element-Cosserat continuum finite element two scale method for granular materials, Journal of the Mechanics and Physics of Solids 122 (2019) 450–471. doi:10.1016/j.jmps.2018.09.029.
URL https://linkinghub.elsevier.com/retrieve/pii/S0022509618301832

[28] H. S. Suh, W. Sun, D. T. O'Connor, A phase field model for cohesive fracture in micropolar continua, Computer Methods in Applied Mechanics and Engineering 369 (2020) 113181. doi:10.1016/j.cma.2020.113181.
URL https://linkinghub.elsevier.com/retrieve/pii/S0045782520303662

[29] M. Ambati, T. Gerasimov, L. De Lorenzis, A review on phase-field models of brittle fracture and a new fast hybrid formulation, Computational Mechanics 55 (2) (2015) 383–405. doi:10.1007/s00466-014-1109-y.
URL http://link.springer.com/10.1007/s00466-014-1109-y

[30] H. Amor, J.-J. Marigo, C. Maurini, Regularized formulation of the variational brittle fracture with unilateral contact: Numerical experiments, Journal of the Mechanics and Physics of Solids 57 (8) (2009) 1209–1229. doi:10.1016/j.jmps.2009.04.011.
URL https://linkinghub.elsevier.com/retrieve/pii/S0022509609000659

[31] Y. Sumi, Z. Wang, A finite-element simulation method for a system of growing cracks in a heterogeneous material, Mechanics of Materials 28 (1-4) (1998) 197–206. doi:10.1016/S0167-6636(97)00048-3.
URL https://linkinghub.elsevier.com/retrieve/pii/S0167663697000483

[32] P. Germain, The Method of Virtual Power in Continuum Mechanics. Part 2: Microstructure, SIAM Journal on Applied Mathematics 25 (3) (1973) 556–575. doi:10.1137/0125053.
URL http://epubs.siam.org/doi/10.1137/0125053

[33] R. De Borst, SIMULATION OF STRAIN LOCALIZATION: A REAPPRAISAL OF THE COSSERAT CONTINUUM, Engineering Computations 8 (4) (1991) 317–332. doi:10.1108/eb023842.
URL https://www.emerald.com/insight/content/doi/10.1108/eb023842/full/html

[34] A. Braides, P. D. o. M. A. Braides, Approximation of Free-Discontinuity Problems, Springer Science & Business Media, 1998, google-Books-ID: 5Ks3FY29MtoC.

[35] T.-T. Nguyen, J. Bolivar, J. Réthoré, M.-C. Baietto, M. Fregonese, A phase field method for modeling stress corrosion crack propagation in a nickel base alloy, International Journal of Solids

and Structures 112 (2017) 65–82. doi:10.1016/j.ijsolstr.2017.02.019.
URL https://linkinghub.elsevier.com/retrieve/pii/S0020768317300744

[36] Accueil | Cast3M.
URL http://132.167.192.71/

[37] S. Forest, Some links between Cosserat, strain gradient crystal plasticity and the statistical theory of dislocations, Philosophical Magazine 88 (30-32) (2008) 3549–3563. doi:10.1080/14786430802154815.
URL http://www.tandfonline.com/doi/abs/10.1080/14786430802154815

[38] M. Nooru-Mohamed, E. Schlangen, J. G. van Mier, Experimental and numerical study on the behavior of concrete subjected to biaxial tension and shear, Advanced Cement Based Materials 1 (1) (1993) 22–37. doi:10.1016/1065-7355(93)90005-9.
URL https://linkinghub.elsevier.com/retrieve/pii/1065735593900059

[39] G. Molnár, A. Gravouil, 2D and 3D Abaqus implementation of a robust staggered phase-field solution for modeling brittle fracture, Finite Elements in Analysis and Design 130 (2017) 27–38. doi:10.1016/j.finel.2017.03.002.
URL https://linkinghub.elsevier.com/retrieve/pii/S0168874X16304954

[40] Y. Okamura, A. Sakashita, T. Fukuda, H. Yamashita, T. T. E. P. C. T. Futami, Tokyo (Japan)], Latest SCC Issues of core shroud and recirculation piping in Japanese BWRs, Vysoka skola technicka, Brno (Czech Republic), International Association for Structural Mechanics in Reactor Technology, Raleigh, NC (United States); Brno University of Technology, Brno (Czech Republic); Czech Association of Mechanical Engineers, Prague (Czech Republic); Czech Technical University, Prague (Czech Republic); Czech Nuclear Society, Prague (Czech Republic); Slovak Nuclear Society, Bratislava (Slovakia), 2003.
URL https://www.osti.gov/etdeweb/servlets/purl/20628417